# PROBABILISTIC MULTI-COMPARTMENTY GEOMETRIC MODEL: APPLICATION TO CELL SEGMENTATION

*S. Farhand*[1], *R.B. Montero*[2], *X. Vial*[2], *D.T. Nguyen*[2], *M. Reardon*[3], *S.M. Pham*[4], *F.M. Andreopoulos*[2,4], *G. Tsechpenakis*[1]

[1]Computer and Information Science Dept., Indiana University-Purdue University Indianapolis, USA

[2]Biomedical Engineering Dept., University of Miami, USA

[3]Biology Department, University of Miami, USA

[4]Daughtry Dept. of Surgery, Miller School of Medicine, University of Miami, USA

## ABSTRACT

We describe a cell segmentation approach based on a probabilistic formulation of multi-compartment level set-based deformable model. We aim at the simultaneous cell partitioning into nucleus and membrane. We consider relative topology of the two distinct cell compartments, while we constrain our solution using shape prior information. Our method integrates geometric models with learning-based classification in a simple graphical model, such that it captures not only the cell compartments but also their topological relationship. We apply our framework to (static) fluorescent microscopy images, where the cultured cells are stained with calcein AM.

***Index Terms***— cell segmentation, multi-compartment geometric model, fluorescent microscopy.

## 1. INTRODUCTION

An important goal in computer and biomedical vision is to transform images into a numerically symbolic form for better representation, evaluation, and/or content-based mining. An essential step in this transformation is the segmentation of target objects/structures.

Cell segmentation in microscopic images is part of our study[1] [5], namely the assessment of the angiogenic effect of growth factor-delivery, as observed in cell proliferation. Existing cell segmentation approaches are based on either deformable and geometric models [10, 4, 1, 3, 6], graph cuts [7], or learning-based pixel/region classification [11]. In [6], Liu et al. combine simple level set segmentation and local graph matching for segmenting and tracking cells in image sequences, using temporal constrains. Wang et al. [10] use wavelet filters to extract dots representing proteins in the cell nucleus, and edges corresponding to membrane boundaries. Then, boosting is used to choose the best features among the filtering results and find the cell centers. The cell region is estimated using a Support Vector Machine on intensity and its gradients. Wang et al. [4] use texture adaptive active contours, taking advantage of the distinct texture of the image around the membrane boundary, in a similar way as in [10]. In the work of [1], shape prior information and edge detection are used in a level set framework. Gelas et al. [3] model the intensity distribution of nuclei with a Gaussian, and use level sets to segment the cell regions.

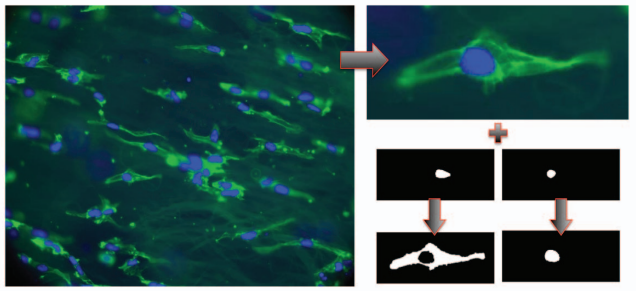


**Fig. 1**: Given a cell image and initial seeds in the nucleus and membrane regions, our task is the segmentation and simultaneous partitioning of the cell into nucleus and membrane. We aim at modeling the cell morphology.

The solution we describe here differs from the existing literature in that (i) we aim at segmenting cells in static images, without considering any temporal changes; (ii) most methods in the literature process grayscale microscopic images, while in our approach we exploit RGB information; (iii) we consider topology constraints of the cell structure for better segmentation; (iv) we integrate region classification with a geometric model; (v) we handle local feature variations by both updating the model interior statistics and employing nucleus-membrane relative topology constraints.

Our goal is to model the cell morphology, i.e., extract shapes and relative topology of nucleus and membrane. This is to assess the effect of biologically responsive scaffolds that deliver multiple angiogenic cytokines and/or cells in ischemic regions [5].

## 2. METHOD

We integrate a region-based geometric model with region classification to combine shape and relative topology in a probabilistic fashion. We build a simple graphical model to solve the joint evolution of two interfaces, namely the nucleus and membrane boundaries (Fig. 3). Since the two compartments are stained in blue and green respectively, we

[1]This work is supported by NIH [#R21EB012136-01]: 'Construction and profiling of biodegradable cardiac patches for the co-delivery of bFGF and G-CSF growth factors', awarded to F.M. Andreopoulos.

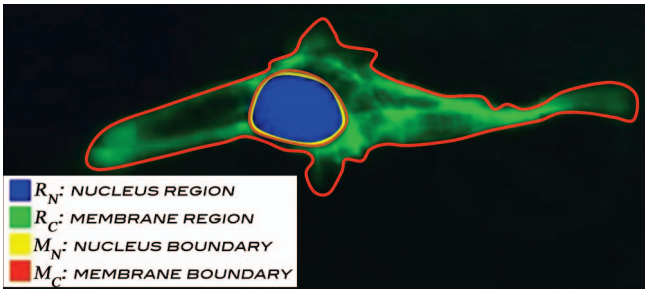



**Fig. 2**: Illustration of $R_N, R_C, M_N, M_C$.

consider these two chromatic components to decompose the input $RGB$ image into the nucleus and membrane images. Initially, we detect those pixels that are more likely to belong to each one of the cell regions, and obtain an initial configuration of the model and the probability field that drives it. For that purpose, we use K-harmonic means clustering [12] with $K \geq 3$, to over-segment the data and calculate the highest pixel memberships to the brightest regions of the two chromatic channels[2]. During evolution, we update the probability field based on the new model position, which enables us to capture local intensity inhomogeneities in the two channels.

Let $I_g(x)$ and $I_b(x)$ be the intensities of the green and blue channel, respectively, at a pixel location with cartesian coordinates $x$ in the image domain $\Omega$, i.e. $\{I_g, I_b\} : \Omega \rightarrow [0,1]$. Also, let $L = \{l(x)\}_{x\in\Omega}$ be the set of pixel labels on the image plane, with $l(x) = \{1,2,3\}$ representing the pixel classes, such that,

$$l(x) = \begin{cases} 1, & x \; in \; nucleus \\ 2, & x \; in \; membrane \\ 3, & otherwise \; (x \; in \; background) \end{cases} \quad (1)$$

Also, let $\hat{\psi}$ be the joint shape for nucleus and membrane, where the individual shapes are modeled with the signed distance functions,

$$\psi_N(x) = \begin{cases} 0, & x \in M_N \\ +d(x, M_N), & x \in R_N \\ -d(x, M_N), & x \in \Omega / R_N \end{cases} \quad (2)$$

for the nucleus region $R_N$ with boundaries $M_N$, and

$$\psi_C(x) = \begin{cases} 0, & x \in M_C \\ +d(x, M_C), & x \in R_C \\ -d(x, M_C), & x \in \Omega / R_C \end{cases} \quad (3)$$

for the membrane region $R_C$ with boundaries $M_C$, as shown in Fig. 2; $d(x, M)$ denotes the (minimum) distance of a point $x$ from the boundary $M$.

Our solution for the estimation of the desired boundaries is based on the graphical model in Fig. 3. To capture relative topology, we implicitly consider that the regions of interest are conditionally dependent and do not overlap in the image domain.

[2]In our experiments, we used K=5. Note that other region classification methods may also be used during initialization.

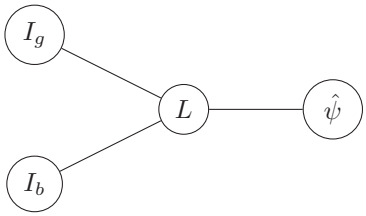



**Fig. 3**: Integration of shape, relative topology, and region classification in a probabilistic graphical model.

### 2.1. Deformable model formulation

Deformable model configuration ($\hat{\psi}$) captures three distinct regions according to appearance, shape, and topology. According to our framework in Fig. 3, our goal is to maximize the joint posterior probability,

$$< \hat{\psi}^*, L^* >= \arg\max_{(\hat{\psi}, L)} P(\hat{\psi}, L|\hat{I}), \quad (4)$$

where $\hat{I} = (I_g, I_b)$, and the objective posterior can be decomposed into,

$$\begin{aligned} P(\hat{\psi}, L|\hat{I}) &= \frac{P(\hat{\psi}).P(L|\hat{\psi}).P(L|\hat{I})}{P(L)} \\ &\propto P(\hat{\psi}).P(L|\hat{\psi}).P(L|\hat{I}) \end{aligned} \quad (5)$$

### 2.2. $P(\hat{\psi})$ : Model prior with relative topology

As explained above, $\hat{\psi}$ consists of the nucleus and membrane shapes $\psi_N$ and $\psi_C$, which are topologically, and therefore conditionally, dependent. Using the chain rule we can obtain two alternatives,

$$\begin{aligned} P(\hat{\psi}) &= P(\psi_N, \psi_C) = P(\psi_N).P(\psi_C|\psi_N) \quad (6) \\ &= P(\psi_C).P(\psi_N|\psi_C) \quad (7) \end{aligned}$$

Because of the intensity smoothness and the low variation in the shape of the nucleus, we constrain the solution for the membrane region using eq. (6).

**A. The prior $P(\psi_N)$.** It is defined as a Gibbs function of the internal energy of $\psi_N$,

$$P(\psi_N) = \frac{1}{Z_{int_N}} exp\{-E_{int_N}\}, \quad (8)$$

where $Z_{int_N}$ is a normalization constant; $E_{int_N}$ encodes the nucleus area, local shape smoothness, and shape prior information, i.e., an approximation of ellipse variations on the image plane,

$$\begin{aligned} E_{int_N} &= \varepsilon_1 A(R_N) + \varepsilon_2 \int\int_{\partial R_N} ||\nabla \psi_N(x)|| dx + \\ &+ \varepsilon_3 Ellipse(R_N), \end{aligned} \quad (9)$$

with $\varepsilon_1, \varepsilon_2$ and $\varepsilon_3$ being the individual term weights, $A(\cdot)$ denoting area, and $\partial R_N$ being a narrow band around the nucleus boundary. Also,

$$Ellipse(R_N) = \frac{R_N \cap R_e^*}{R_N \cup R_e^*}, \quad (10)$$

where $R_e^*$ is the region enclosed by the ellipse that best fits the nucleus boundaries.

The minimization of $E_{int_N}$ forces the nucleus interface towards a locally smooth form, with minimum enclosed area and maximum similarity with an ellipse (minimum fitting error).

**B. The likelihood $P(\psi_C|\psi_N)$.** The second term of eq. (6) encodes relative topology between nucleus and cell membrane. We model this term using the concept of *joint parts* [2], which are regions determined by adjacent parts of the target. We use this concept to impose the constraints: (a) a nucleus is surrounded by membrane, (b) the existence of the two compartments is mutually inclusive. According to [2], a multi-region distance function is defined,

$$\varphi_J = \max\{\psi_N, 0\} + \max\{\psi_C, 0\} + \max\{\psi_B, 0\}, \quad (11)$$

where $\psi_B$ is the distance function defined for the background $B$ in a similar way as in eqs. (2),(3).

To facilitate notion, let $(i, j)$ index any pair of distinct regions of interest $O$: $O_{i\ or\ j} = \{R_N, R_C, B\}$, where, following the label assignments of eq. (1), $(i, j) = \{1, 2, 3\}, i \neq j$. The multi-region distance $\varphi_J$ is nonzero at every location $x \in \Omega$ except for the interfaces $\{M_N, M_C\} = b_{ij} = \partial(O_i \cap O_j)$. The joint part between any pair $(O_i, O_j)$ is,

$$J_{ij} = \{x \ \epsilon \ O_i \cup O_j \ \mid \min_{y \epsilon b_{ij}} ||x - y|| < \min_{z \epsilon B_{ij}} ||x - z||\}, \quad (12)$$

where $B_{ij}$ is the boundary of $O_i \cup O_j$. Intuitively, if $x \in J_{ij}$, then $x$ is closer to the shared boundary than the boundary of the union. Also, the notion of the *first neighbor* is introduced to define the label function,

$$f(x) = j, \qquad if \ \ x \ \epsilon \ O_i \cap J_{ij}, \ \forall (i, j) \in [1, 3], i \neq j, \quad (13)$$

i.e.,

$$x \in J_{ij}, \ if \ \{l(x), f(x)\} = \{i, j\} \ or \ \{j, i\} \quad (14)$$

Finally, the distance,

$$\varphi_f = \sum_{i,j=1, i \neq j}^{3} \max\{\psi_{ij}, 0\} - \max\{\psi_i, \psi_j, 0\}, \quad (15)$$

is considered, where $\psi_{ij}$ is the distance function of $O_i \cup O_j$, and $\psi_{i\ or\ j} = \{\psi_N, \psi_C, \psi_B\}$.

Following the definitions above, the topology and shape of the cell can be modeled in the image domain by the functions $\varphi_J$ and $\varphi_f$, and the individual shapes can be recovered by,

$$\psi_i(x) = \begin{cases} \varphi_J, & \text{if } l(x) = i \\ -\varphi_J, & \text{if } l(x) \neq i \text{ and } f(x) = i \\ -\varphi_J - \varphi_F, & \text{if } l(x) \neq i \text{ and } f(x) \neq i \end{cases} \quad (16)$$

Fig. 4 illustrates the joint parts and the boundaries $M_N$, $M_C$ at three instances $(t_1, t_2, t_3)$ during evolution. Notice that at $t_1$, the joint part $J_{NC}$ (nucleus-cytoplasm) is zero since the two regions are not adjacent; similarly, for nucleus-background at $t_3$, it is $J_{NB}(x) = 0, \forall x \in \Omega$.

Using these definitions we can formulate the internal energy function of the membrane model $\psi_C$ as,

$$E_{int_C} = \varepsilon_4 A(R_C) + \varepsilon_5 \int\int_{\partial R_C} ||\nabla \psi_C(x)|| dx + \varepsilon_6 \frac{A(J_{NB})}{A(J_{NC})}, \quad (17)$$

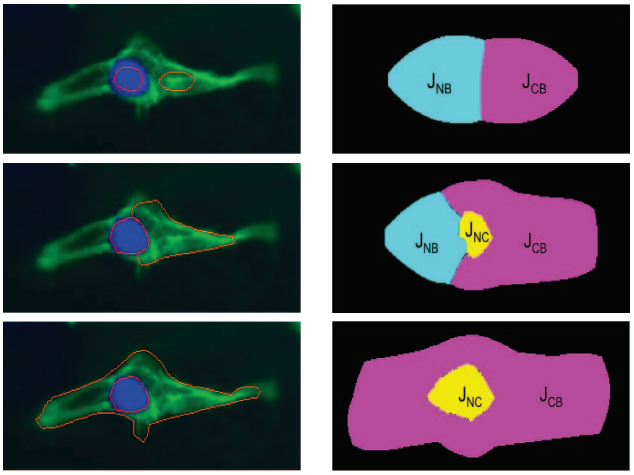



**Fig. 4**: Left: model evolution at three instances ($t_1 < t_2 < t_3$); right: corresponding changes to the joint parts.

where $\varepsilon_4, \varepsilon_5$ and $\varepsilon_6$ are the individual term weights. The minimization of this energy, in a similar way as eq. (9), enforces minimum area and maximum local shape smoothness, while the last term forces the membrane region to surround (grow around) the nucleus (Fig. 4). Then, the joint topology likelihood of eq. (6) is,

$$P(\psi_C|\psi_N) = \frac{1}{Z_{int_C}} exp\{-E_{int_C}\}, \quad (18)$$

with $Z_{int_c}$ being a normalization constant.

### 2.3. $P(L|\hat{\psi})$: dependency model-class assignments

In the decomposition of our objective in eq. (5), we model the dependency between the model configuration and the estimated label field using sigmoid functions $g(\cdot)$, in a similar way as in [9],

$$\begin{cases} P(L = 1|\hat{\psi}) = \frac{g(\psi_N)}{G} \\ P(L = 2|\hat{\psi}) = \frac{g(\psi_C)}{G} \\ P(L = 3|\hat{\psi}) = \frac{g(-\max(\psi_N, \psi_C))}{G} \end{cases} \quad (19)$$

where $G = g(\psi_N) + g(\psi_C) + g(-\max(\psi_N, \psi_C))$.

### 2.4. $P(L|\hat{I})$: image label field

The last term of our objective in eq. (5) is the probability of class assignments to the pixels. For its estimation we use binary Support Vector Machine classification on pixel intensities in each of the two grayscale images $I_g$, $I_b$. The SVM calculates the decision approximation functions, and the probabilities $P(L|I_g)$, $P(L|I_b)$ are estimated using the log maximum likelihood approach of [8]. Then, it is $P(L|\hat{I}) = P(L|I_g).P(L|I_b)$, assuming conditional independence between the two chromatic channels. During evolution, the probability field is updated, and the new labels drive the model dynamics.

## 3. EXPERIMENTAL RESULTS

We tested our method using a set of 50 single-cell images, manually cropped from 20 cell cultures. Although the simul-

taneous segmentation of all cells ($\sim 5-40$ in each culture) can be achieved using multiple models, our goal here is to demonstrate the cell partitioning into nucleus and membrane, which is crucial in our application[3].

Fig. 5 illustrates some indicative results of our method. In some cases with minimum photo-bleaching, the initialization for the nucleus and/or membrane regions is very close to the desired boundaries. Therefore, to show the scalability of our approach, we manually chose seeds among the regions that are initially assigned to corresponding classes by the K-harmonic means clustering. In all examined images, our model correctly captures $> 97\%$ of the nucleus, with $< 2\%$ of its area false positive assignments, and $> 91\%$ of the membrane, with $< 4\%$ of the its area false positives. Due to topology constraints we impose between the two compartments, during evolution the estimated membrane region does not *leak* at the sites where the photo-bleaching degree is high.

One obvious issue in our model is the selection of the weights $\{\varepsilon_1, \varepsilon_2, \varepsilon_3\}$ in eq. (9) and $\{\varepsilon_4, \varepsilon_5, \varepsilon_6\}$ in eq. (17). Fig. 5 shows the weight choices we made for these examples. Empirically, the weights of the ellipse fitting term in eq. (9) and the joint topology term in eq. (17), $\varepsilon_3$, $\varepsilon_6$ respectively, are assigned higher values in cases of increased noise.

## 4. CONCLUSIONS AND FUTURE WORK

We presented a probabilistic multi-compartment geometric model for the segmentation and simultaneous partition of cells into their nucleus and membrane regions. We tested our method using fluorescent microscopy images, where the two region classes are distinguished by color. An obvious extension of our method is its application to different modalities, e.g., grayscale images where the target parts have different intensity distributions or higher-scale texture patterns. We use our approach to study the cell morphology as outcome of a growth factor (cytokine) delivery procedure. Our future work includes the integration of our framework into a unified optimization approach, where classification and deformable model parameters will be estimated using an L1-norm logistic classification in a Max-product procedure.

## 5. REFERENCES


[1] T. Chen, Y. Zhang, C. Wang, Z. Qu, M. Cai, F. Wang, and T. Syeda-Mahmood, 'Local complex phase based level set and its application to DIC red blood cell segmentation,' *ISBI*, 2011.

[2] X. Fan, P.L. Bazin, and J. L. Prince, 'A multi-compartment segmentation framework with homeomorphic level sets,' *CVPR*, 2008.

[3] A. Gelas, K. Mosaliganti, A. Gouaillard, L. Souhait, R. Noche, N. Obholzer, and S. Megason, 'Variational level- set with gaussian shape model for cell segmentation,' *ICIP*, 2009.

[4] W.He,X.Wang,D.Metaxas,R.Mathew,and E.White, 'Cell segmentation for division rate estimation in computerized video time-lapse microscopy,' *Soc. of Photo-Optical Instrumentation Engineers (SPIE) Conf. Series*, Mar. 2007.

[5] H. Layman, X. Li, E. Nagar, A. Azar, S.M. Pham, G. Tsechpenakis, and F.M. Andreopoulos, 'Synergistic angiogenic effect of co-delivering FGF-2 and G-CSF from fibrin scaffolds and bone marrow transplantation in critical limb ischemia,' *Tissue Engineering*, Part A, 17(1-2), pp. 243-254, 2011.

[6] F. Li, X. Zhou, H. Zhao, and S. T. Wong, 'Cell segmentation using front vector flow guided active contours,' *MICCAI*, 2009.

[7] M. Liu, A. Roy-Chowdhury, and G. Venugopala Reddy, 'Robust estimation of stem cell lineages using local graph matching,' *CVPR*, 2009.

[8] J.C. Platt, 'Probabilistic outputs for Support Vector Machines and Comparisons to Regularized Likelihood Methods,' Advances in Large Margin Classifiers, A. Smola, P. Bartlett, B. Schlkopf, D. Schuurmans (Eds.), pp. 61-74, MIT Press, 1999.

[9] G. Tsechpenakis and D. N. Metaxas, 'CRF-driven implicit deformable model,' *CVPR*, 2007.

[10] X.Wang,W.He,D.Metaxas,R.Mathew,and E.White ',Cell segmentation and tracking using texture-adaptive snakes,' *ISBI*, 2007.

[11] Z. Yin, R. Bise, M. Chen, and T. Kanade, 'Cell segmentation in microscopy imagery using a bag of local bayesian classifiers,' *ISBI*, 2010.

[12] B. Zhang, 'Generalized K-Harmonic Means - Boosting in Unsupervised Learning,' *Technical Report HPL-2000-137*, Hewlett-Packard Labs, 2000.

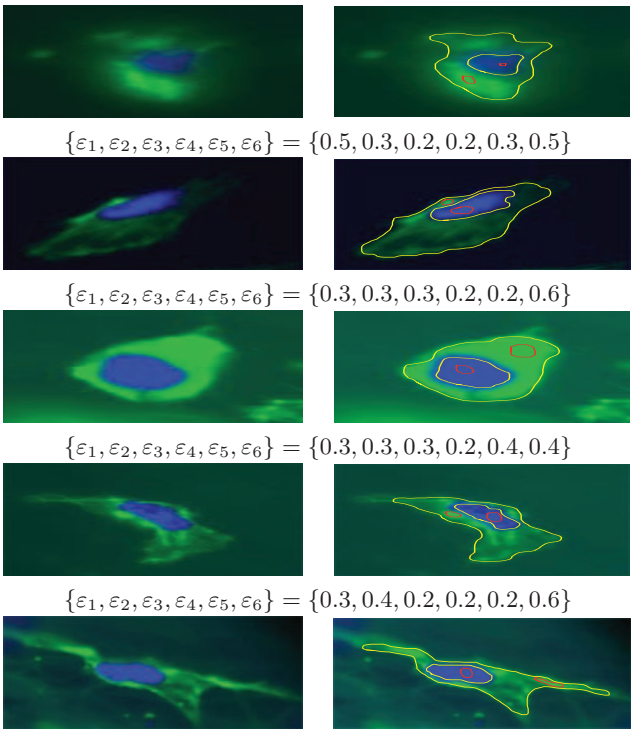




**Fig. 5**: Segmentation results. (a) Original images. (b) Initializations in membranes and nuclei (red lines), and final results (yellow lines).

[3] Here we do not aim to solve the problem of segmenting cells that are in close proximity or adjacent to each other.